Effect of filling configurations on melting heat transfer characteristic of phase change materials partially filled with metal foam

Hui Wang, Qifan Ying, Eric Lichtfouse, Zexu Hu, Yongfa Diao

Journal of Energy Storage 69 (2023) 107858

https://doi.org/10.1016/j.est.2023.107858

Effect of filling configurations on melting heat transfer characteristic of phase change materials partially filled with metal foam

Hui Wang [a,*], Qifan Ying [a], Eric Lichtfouse [c], Zexu Hu [b], Yongfa Diao [a]

[a] College of Environmental Science and Engineering, Donghua University, Shanghai 201620, China
[b] State Key Laboratory for Modification of Chemical Fibers and Polymer Materials, Donghua University, Shanghai 201620, China
[c] Aix Marseille Univ, CNRS, IRD, INRAE, CEREGE, Aix-en-Provence, France

ARTICLE INFO

Keywords:
Thermal energy storage
Phase change materials
Metal foam
Partially filled
Heat transfer enhancement

ABSTRACT

Metal foam embedded in phase change materials (PCM) has been shown to significantly improve the storage of latent heat thermal energy. Nonetheless the presence of metal foam also reduces natural convection, energy storage and increases cost. To address this issue, we modelled the internal flow of heat transfer in a PCM, paraffin wax, filled with metal foam at the top or the bottom, with filling height ratio ξ of 0.25, 0.5 and 0.75. The liquid-solid phase transition was studied by numerical simulations. Results show that natural convection in the pure paraffin wax area is higher, and melting time is shorter, in the bottom-filled than in the top-filled configuration. These differences increase with filling height ratio. By contrast, in metal foam-paraffin composite region, melting time is longer in the bottom-filled configuration due to heat loss. Interestingly, we observed significant changes in the interface shape of liquid-solid PCM at the junction of the pure paraffin and the metal foam-paraffin composite region. The liquid fraction formulas for different metal foam filled configurations are established as the function of Fourier number, Rayleigh number and filling height ratio.

1. Introduction

Storing energy and using energy efficiently have become research hotspots in the context of the rising energy demand and the global fuel crisis [1,2]. In particular, latent heat thermal energy storage (LHTES) using PCM is promising because these materials store high amounts of energy storage within a small temperature difference [3]. In solar energy storage system, PCM decrease intermittency and uneven spatial distribution [4,5]. In electronics, PCM absorb large amounts of heat emanating from electronic components, thus prevent heat damage [6,7].

PCM can be organic, mineral or eutectic mixtures. Compared to minerals, organic materials display better properties such as non-corrosive, no phase segregation, and super cooling [8]. However, due to their low thermal conductivity, application of purely organic materials is limited. Two main methods allow to enhance the heat transfer of phase-change materials: material modification [9,10] or adding strengthening additives, such as fins [11,12], nanoparticles [13,14], graphene [15,16], metal foam [17,18], and carbon nanotubes [19,20]. In particular, metal foams display advantages such as small density, high surface area, high thermal conductivity and good wettability for PCM. As a consequence, metal foam-phase change material composites show enhanced heat transfer capability [21–25].

Nonetheless, the high porosity of metal foams induces limitations in composites. For instance, Zhang et al. [26] numerically pointed out that metal foam could increase the overall heat transfer rate of paraffin by 3–10 times, but the porous characteristics of metal foam inhibited the natural convection effect of paraffin. Li et al. [27] also found experimentally that metal foam induces a high resistance to liquid paraffin, and that natural convection is more inhibited at higher pore density, thus leading to an uneven temperature distribution along paraffin flow. Moreover, the global latent heat is decreased due to the lower mass of paraffin in the composite, versus pure paraffin. Yao et al. [28] experimentally found that the flow of liquid paraffin with metal foam is hindered by the porous structure, and the flow resistance increases with the decrease of pore size. Tao et al. [29] found numerically that increasing the pores per inch (PPI) of metal foam enhances the thermal conductivity of phase-change materials, but highly inhibits the natural convection of paraffin. Meng et al. [30] found that when the porosity of copper foam is reduced from 0.98 to 0.88, the melting time is shortened by 68.7 %, but 22.3 kJ heat storage is lost for every 2 % porosity reduction.

As the fully filled metal foam has obvious deficiency, partially filled

* Corresponding author.
E-mail address: huiwang@dhu.edu.cn (H. Wang).

configuration has been proposed. In the experimental study of Zhang et al. [31], it was found that when the metal foam filling ratio was 5/6, the melting rate and thermal storage efficiency reached the maximum, which was better than the case of full filling. Liu et al. [32] observed the melting process of paraffin without metal foam filling and three different locally filled structures through experiments, and found that different filling structures had a great influence on the phase transition rate, so it was important to obtain the prediction formula of liquid fraction. Zhu et al. [33] compared the influence of metal foam content on the transient performance of paraffin/copper foam radiators through experiments, and found that it was more economical to fill copper foam locally with 2/3. Hou et al. [34] experimentally studied the effect of horizontal local filling of metal foam on the heat thermal storage process of paraffin, and found that horizontal local filling could not only improve the melting rate, but also avoid the significant reduction of heat storage.

In numerical research, Zuo et al. [35] numerically studied the effect of metal foams with different filling angles and thicknesses on the melting performance of phase-change materials. When the filling angle is >150°, the melting rate does not increase significantly, so overfilling is not necessary. And increasing the thickness will increase the material cost, but reducing the thickness will cause the loss of heat transfer performance. Yang et al. [36] numerically compared the heat transfer process of shell-and-tube heat exchangers with different metal foam filling rates. Results demonstrate that filling ratio lower than 0.85 does not increase heat transfer enhancement. When the filling rate is 0.89, the melting time is the shortest, which is 10 % shorter than that of the fully filled configuration, but the temperature distribution is extremely uneven at this time. Wang et al. [37] examined the effect of the filling rate of copper foam on the melting process of paraffin when the bottom filling configuration was adopted through experiments and numerical simulations. The filling rate of copper foam increased from 0 % to 2.13 %, the paraffin melting accelerated for 110 s, and the temperature gradient decreased from 30.9 K to 5.2 K. More filling rate made the temperature distribution of the composite more uniform. With the increase of filling rate, the natural convection is weakened more seriously, and the heat storage is also reduced. Joshi et al. [38] also analyzed the situation of metal foam filling at the bottom, and the simulation results showed that the melting time of PCM was shortened, but at the cost of heat storage. Taking the time to reach 90 % heat storage of pure phase-change materials as the index, the authors found that the filling height ratio of 0.75 and 1 cases took the same time, and considered that using a filling height ratio of >0.75 is not worthy.

Overall, partially filled metal foam have been widely studied as a means of improving heat transfer during PCM melting. However, the current research on the flow and heat transfer characteristics of PCM in partially reinforced configuration systems is not comprehensive, especially with respect to different filling configurations, remains elusive. Furthermore, the prediction of liquid fraction for PCM melting in such systems has not been fully investigated. In this paper, we studied numerically systems that were partially filled with metal foam, in two configurations: top filling and bottom filling. The liquid-solid interface development, temperature response and liquid fraction under different filling configurations were compared and analyzed to obtain the flow heat transfer characteristics of PCM melting process. In addition, the liquid fraction prediction formulas for different configurations are established. Notably, this prediction formula can be applied beyond the scope of this study, offering potential for predicting the liquid fraction in other geometries. Our study may provide ideas for the design of efficient LHTES systems.

Nomenclature

A_m	Mushy coefficient	λ	thermal conductivity (W m^{-1} K^{-1})
c_p	Specific heat capacity ($J{\cdot}kg^{-1}{\cdot}K^{-1}$)	μ	dynamic viscosity ($kg{\cdot}m^{-1}{\cdot}s^{-1}$)
C_i	form coefficient (m^{-1})	ρ	density ($kg{\cdot}m^{-3}$)
d_f	fiber diameter (m)	ξ	height ratio of metal foam
d_p	pore size (m)	δ	small constant number
d_k	characteristic length (m)	χ	tortuosity coefficient
g	acceleration of gravity ($m{\cdot}s^{-2}$)	ω	pores per inch (m^{-1})
grad	gradient	Subscripts	
H_{mf}	metal foam height (m)	*0*	initial time
K	permeability (m^2)	*co*	composite
L	characteristic length (m)	*eff*	effective value
L_a	latent heat of fusion ($kJ{\cdot}kg^{-1}$)	*i*	position along the interface
n	number of segments	*pcm*	phase change material
q	heat flux (W m^{-2})	*m*	melting point
S	source term	*mf*	metal foam
t	time (s)	*l*	liquid state
t^*	dimensionless time	*la*	latent heat
t_m	melting time (s)	*s*	solid state
T	temperature (K)	*se*	sensible heat
u, v	x, y direction velocity ($m{\cdot}s^{-1}$)	*w*	wall
W	LHTES unit width (m)	Abbreviations	
x, y	Cartesian coordinates (m)	*BTC*	bottom filling configuration
Greek symbols		*LHTES*	latent heat thermal energy storage
α	thermal diffusivity ($m^2{\cdot}s^{-1}$)	*PCM*	phase change material
β	liquid fraction	*PPI*	pores per inch (m^{-1})
γ	thermal expansion coefficient (K^{-1})	*TFC*	top filling configuration
ε	porosity		

2. Physical model and numerical approach

2.1. Physical model

Physical models of the different filling configurations in this study are shown in Fig. 1. The model is a two-dimensional, 90 mm height (H), 60 mm width (W) rectangle filled with different amounts of PCM and metal foam according to different configurations. Paraffin wax was chosen as PCM in this study due to its high latent heat and stable chemical properties, and copper was selected for metal foam because of its high thermal conductivity. The thermophysical properties and structural parameters of paraffin wax and copper foam are listed in Table 1.

The left wall in red is the heating surface, and the remaining black lines represent the adiabatic walls. The pure paraffin and the metal foam-paraffin composite regions appear in plain grey and orange-black, respectively. Two types of configurations are designed: the top filling configuration (TFC) (Fig. 1(a)–(c)), where metal foam is at the top, and the bottom filling configuration (BFC), where metal foam is at the bottom (Fig. 1(d)–(f)). The height ratio of metal foam is defined by $\xi = H_{mf}/H$, where H_{mf} is the filling height of metal foam. The ξ of case T1, T2 and T3 are 0.25, 0.5 and 0.75, respectively. The ξ of B1, B2 and B3 are 0.25, 0.5 and 0.75, respectively. Fig. 1g and h show pure paraffin filling ($\xi = 0$) and full metal foam-paraffin filling ($\xi = 1$). To obtain detailed information about the melting process in each region, four monitoring points O_1, O_2, O_3 and O_4 were set along the center line of the model, as shown in Fig. 2, which were located at heights of 11.25, 33.75, 56.25 and 78.75 mm from the bottom.

2.2. Equations

To study the liquid-solid phase change within metal foams, enthalpy porosity and volume averaging are employed to construct our numerical model, with the following assumptions: 1) The liquid PCM is considered incompressible and moves laminar. 2) Its buoyancy follows the Boussinesq approximation and ignores the volume expansion of paraffin. 3) PCM and metal foam are isotropic. 4) The thermophysical properties of PCM and metal foam are constant with time, and they maintain a local thermal equilibrium. Accordingly, the equations are [31]:

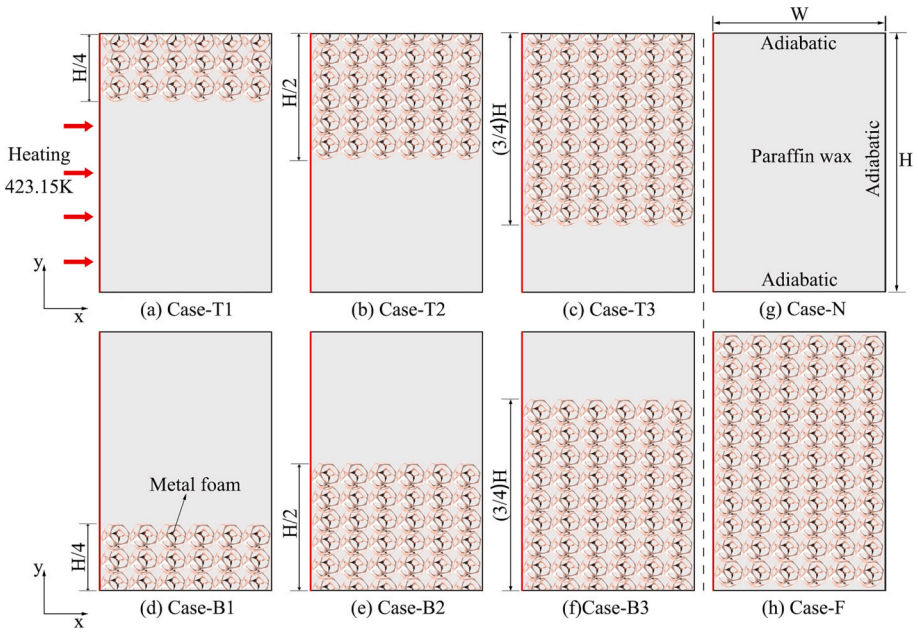

Fig. 1. Physical model of different configurations of metal foam in metal foam-paraffin systems.

Table 1
Thermo-physical properties of paraffin and copper foam.

	Paraffin	Copper
Density (kg·m^{-3}) (solid/liquid)	800/760	8930/–
Specific heat capacity (J·kg^{-1}·K^{-1}) (solid/liquid)	1800/2000	386/–
Thermal conductivity (W·m^{-1}·K^{-1})	0.24	398
Latent heat (kJ·kg^{-1})	250	–
Dynamic viscosity (kg m^{-1}·s^{-1})	2.508×10^{-3}	–
Thermal expansion coefficient (K^{-1})	7.5×10^{-4}	–
Melting temperature range (K)	318.15–328.15	–
Porosity/density	–	0.9/10PPI

Continuity equation:

$$\frac{\partial \rho_{pcm}}{\partial t} + \rho_{pcm}\left(\frac{\partial u}{\partial x} + \frac{\partial v}{\partial y}\right) = 0 \tag{1}$$

Momentum equations:

$$\frac{\rho_{pcm}}{\varepsilon}\left(\frac{\partial u}{\partial t} + \frac{1}{\varepsilon}\left(\frac{\partial (uu)}{\partial x} + \frac{\partial (uv)}{\partial y}\right)\right) = -\frac{\partial p}{\partial x} + \frac{\mu_{pcm}}{\varepsilon}\left(\frac{\partial^2 u}{\partial x^2} + \frac{\partial^2 u}{\partial y^2}\right) + S_x \tag{2}$$

$$\frac{\rho_{pcm}}{\varepsilon}\left(\frac{\partial u}{\partial t} + \frac{1}{\varepsilon}\left(\frac{\partial (vu)}{\partial x} + \frac{\partial (vv)}{\partial y}\right)\right) = -\frac{\partial p}{\partial y} + \frac{\mu_{pcm}}{\varepsilon}\left(\frac{\partial^2 v}{\partial x^2} + \frac{\partial^2 v}{\partial y^2}\right) + S_y \tag{3}$$

where, ε is porosity, an important structural parameter of metal foam, defined as the ratio of pore volume to metal skeleton volume. The last term on the right side of Eqs. (2) and (3) is defined as the source term in x and y directions, respectively, which can be obtained from the following formula:

$$S_x = -\frac{(1-\beta)^2}{\beta^3 + \delta} A_m u - \left(\frac{\mu_{pcm}}{K} + \frac{\rho_{pcm} C_i}{\sqrt{K}} |u|\right) u \tag{4}$$

$$S_y = -\frac{(1-\beta)^2}{\beta^3 + \delta} A_m v - \left(\frac{\mu_{pcm}}{K} + \frac{\rho_{pcm} C_i}{\sqrt{K}} |u|\right) v + \rho_{pcm} g \beta \left(T_{pcm} - T_0\right) \tag{5}$$

where the first term of S_x and S_y represents the flow resistance in the mushy zone when the PCM is melted. In this work, the coefficient A_m of the mushy zone is set equal to 10^5 [39,40]. In addition, a constant denoted as $\delta(0.001)$ is introduced to prevent the denominator from being zero. The remaining terms of S_x and S_y represent the influence of metal foam on the momentum equation, including viscosity, inertia resistance and buoyancy. The parameters related to metal foam, calculated by semi-empirical correlations in the literature, have been shown in Table 2.

Energy equation:

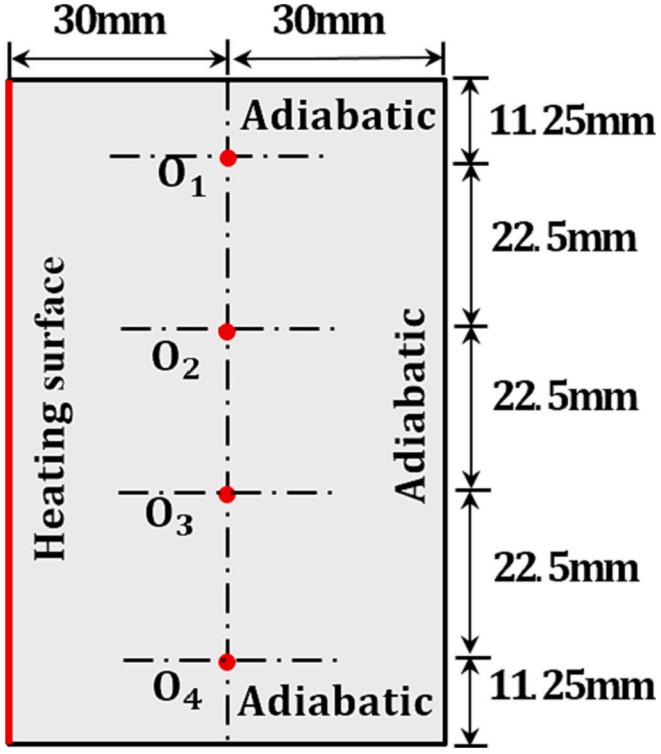

Fig. 2. Position of monitoring points.

Table 2
Semi-empirical correlations for metal foam parameters.

Parameter	Correlation	Reference
Liquid fraction, β	$\beta = \begin{cases} 0 & T_f \le T_{m1} \\ (T_f - T_{m1})/(T_{m2} - T_{m1}) & T_{m1} \le T_f \le T_{m2} \\ 1 & T_{m2} \le T_f \end{cases}$	Xiao et al. [41]
Permeability, K	$K = \frac{(\varepsilon d_k)^2}{36\chi(\chi - 1)}$	Fourie et al. [42]
Tortuosity coefficient, χ	$\chi = 2 + 2cos\left(\frac{4\pi}{3} + \frac{1}{3}cos^{-1}(2\varepsilon - 1)\right)$	
Characteristic length, d_k	$d_k = \frac{\chi}{3 - \chi} d_p$	
Pore size, d_p	$d_p = \frac{22.4 \times 10^{-3}}{\omega}$	
Inertial coefficient, C_i	$C_i = 0.00212(1 - \varepsilon)^{-0.132}\left(\frac{d_f}{d_p}\right)^{-1.63} / \sqrt{K};$	Calmidi et al. [43]
Fiber diameter, d_f	$d_f = 1.18\sqrt{\frac{(1 - \varepsilon)}{3\pi}} d_p$	

$$\left[(1-\varepsilon)(\rho c_p)_{mf} + \varepsilon(\rho c_p)_{pcm}\right]\frac{\partial T}{\partial t} + (\rho c_p)_{pcm}\left(u\frac{\partial T}{\partial x} + \frac{\partial T}{\partial y}\right) = \lambda_{eff}\left(\frac{\partial^2 T}{\partial x^2} + \frac{\partial^2 T}{\partial y^2}\right) - \varepsilon\rho L\frac{\partial \beta}{\partial t} \tag{6}$$

The subscripts mf and pcm represent the metal foam and phase change material respectively, and λ_{eff} is the effective thermal conductivity of metal foam phase-change material composite, which is calculated by the model proposed by Bhattacharya [44]:

$$\lambda_{eff} = 0.35\left(\varepsilon\lambda_{pcm} + (1-\varepsilon)\lambda_{mf}\right) + \frac{0.65}{\left(\frac{\varepsilon}{\lambda_{pcm}} + \frac{1-\varepsilon}{\lambda_{mf}}\right)} \tag{7}$$

2.3. Boundary and initial conditions

The computational domain is shown in Fig. 1. At the initial time, the temperature of each filling configuration model is equal to the ambient temperature, and the initial velocity in x and y directions is zero, as shown in Eq. (8). The left wall is an isothermal heating surface, and the other walls are defined as adiabatic, as shown in Eq. (9).

$$t = 0, T_0 = 293.15K; u = v = 0 \tag{8}$$

$$T|_{x=0m} = 423.15K, \frac{\partial T}{\partial x}\Big|_{x=0.06m} = \frac{\partial T}{\partial x}\Big|_{y=0m}\frac{\partial T}{\partial x}\Big|_{y=0.09m} = 0 \tag{9}$$

2.4. Numerical procedure

The discretization of the governing equations is based on the finite volume method (FVM) and the double-precision solver. The meshing of the computational domain is depicted in Fig. 3. The SIMPLE algorithm was used for pressure-velocity coupling, and the pressure correction equation is discretized by the PRESTO method.

3. Independence tests and model validation

3.1. Independence tests

In order to take into account the error caused by the number of grids and time steps on the simulation results, this study carried out an independence analysis on cases with different grid numbers and time steps before model validation, in order to optimize the appropriate grid number and time step. In the tests, the case with fully filled copper foam was selected for simulation, and the material parameters, boundary and initial conditions are shown in Table 1 and Eqs. (8)–(9) respectively.

Four sets of mesh models with 5400, 15,000, 33,750, and 86,400 elements were tested, with a time step of 0.2 s in each case. The grid specifications are shown in Table 3. Simulation results of melting time with different grid numbers are shown in Fig. 4(a). It can be seen that with the increase of the grid number, the melting time increases and tends to be constant. Although the grid number increases twice from 33,750 to 86,400 elements, the melting time is the same. From the liquid fraction variation, the curves of the four mesh models are approximately coincided, and the maximum deviation of the gird number of 33,750 and 86,400 is only 1 %. Considering the calculation cost and accuracy, the number of grid is set as 33,750. Further, after having fixed the grid number, this study conducted independent analysis on cases with time steps of 2 s, 1 s, 0.2 s and 0.1 s. The melting time at different time steps is presented in Fig. 5(a). Convergence can be achieved under each time step. When the time step is 0.2 s, the melting time is only 1.1 %, more than that of 0.1 s, and the maximum deviation of liquid fraction is 1.6 %. Therefore, it is sufficient to select 0.2 s as the time step. In conclusion, 33,750 was finally chosen as the optimum grid number, and the corresponding time step is 0.2 s.

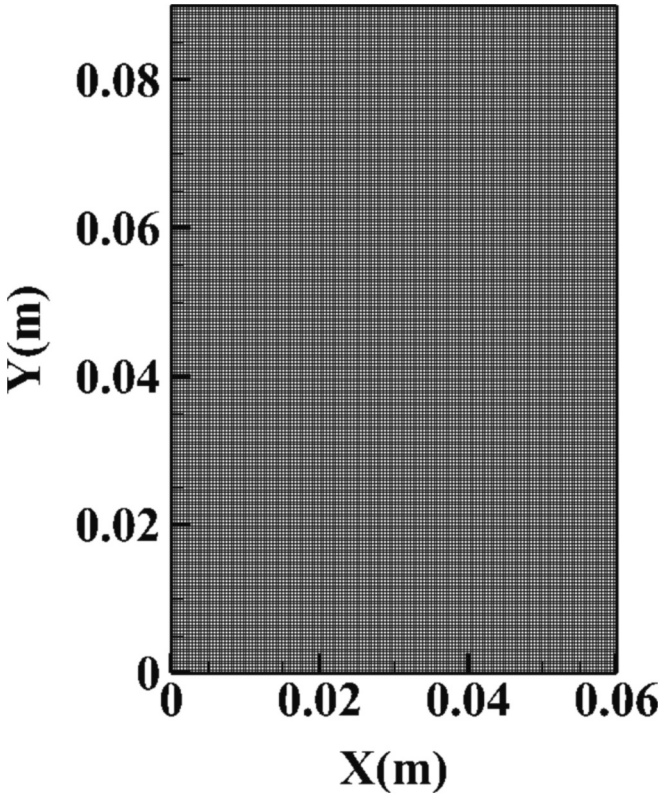

Fig. 3. Meshing system (ξ = 1).

3.2. Model validation

To test the accuracy of the numerical model of PCM melting heat transfer in porous media, the numerical simulation of this work was compared with simulation results of Zheng et al. [45], and the experimental results of Li et al. [46]. Firstly, a square cavity of 60 mm × 60 mm was constructed and uniformly filled with paraffin and metal foam. Then, four different operating conditions are simulated on this basis, and

Table 3
Grid specifications for grid independence tests.

	Value			
Grid number	5400	15,000	33,750	86,400
Specifications	60(*x*) × 90 (*y*)	100(*x*) × 150 (*y*)	150(*x*) × 225 (*y*)	240(*x*) × 360 (*y*)

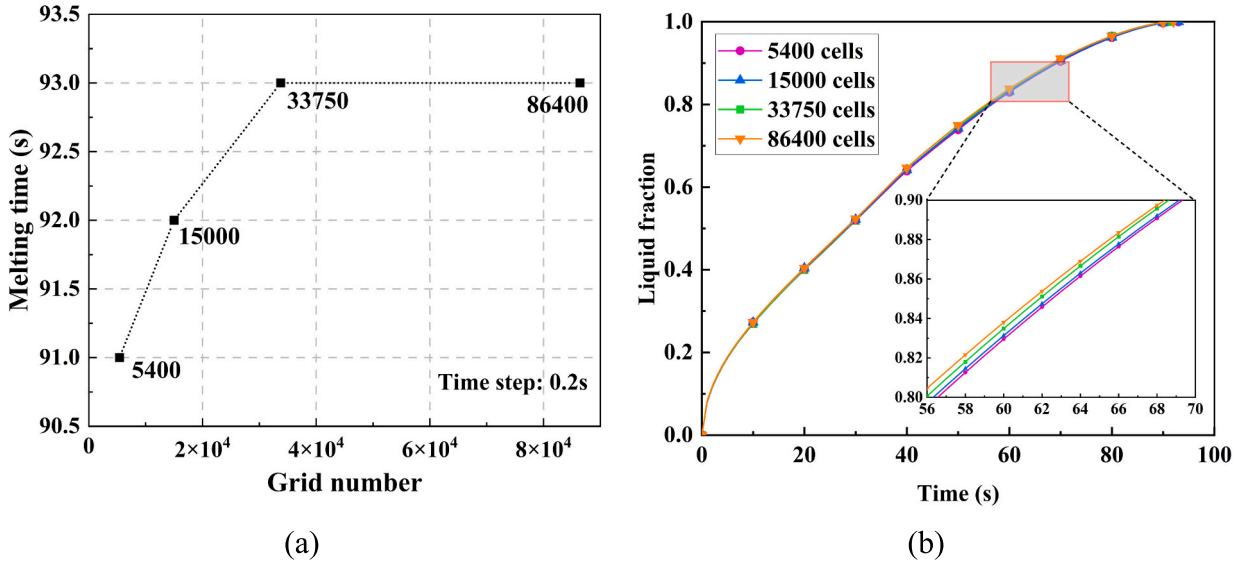

Fig. 4. Comparison of melting time (a) and liquid fraction (b) under different grid number.

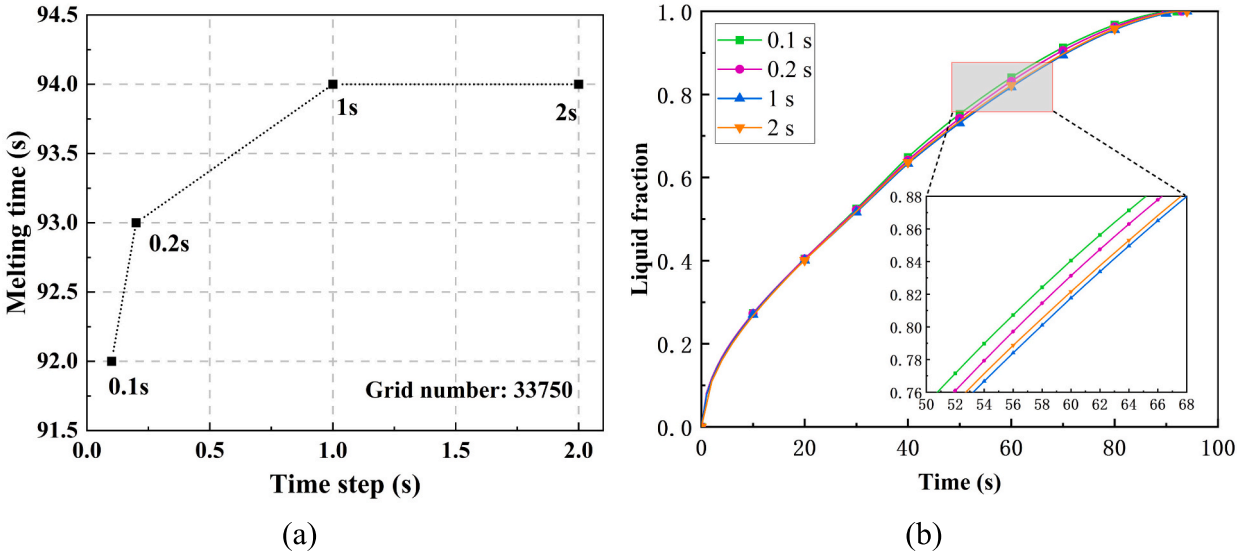

Fig. 5. Comparison of melting time (a) and liquid fraction (b) under different time step.

the specific parameters are listed in Table 4. Finally, the comparison results are shown in Fig. 6(a). We observe that simulation results under different operating conditions are in good agreement with literature simulation. The maximum error of the liquid fraction under the four operating conditions is 3.05 %, indicating that our numerical model is reliable.

In addition, the present numerical results are compared with previous experimental results. A three-dimensional model with a monitoring point was established (Fig. 6(b)). Parameters of paraffin and metal foam were set in accordance with the literature. The initial time of the system was in an ambient temperature of 299.15 K, and a constant heat flow of 4000 W/m^2 was applied to the left wall. The results show that the maximum deviation is only 1.5 %, which is close to the experimental results, and also proves the reliability of the numerical approach in this study.

Table 4
Operating parameters involved in model validation.

	Case-1	Case-2/3/4
Material of metal foam	Nickel	Aluminum
Porosity/density	0.9/10PPI	0.95/10PPI
Heating surface	Left wall	Bottom wall
Heating temperature (K)	350	350, 400, 450
Remaining wall	Adiabatic	Adiabatic

4. Results and discussion

4.1. Fully filled systems

Figs. 7 and 8 show the progression of the liquid-solid interface with time for the system containing solely the PCM (paraffin), with height ratio ξ of 0, and the system fully filled with metal foam in the phase-change material, with ξ of 1. $\beta = 0.5$ (corresponding temperature 323.15 K) is used to evaluate the liquid-solid interface on the right of Figs. 7 and 8, representing half of the liquid-solid region. For pure paraffin, the liquid-solid interface develops initially at the top and left. This can be explained by the lower density of the liquid, and heat

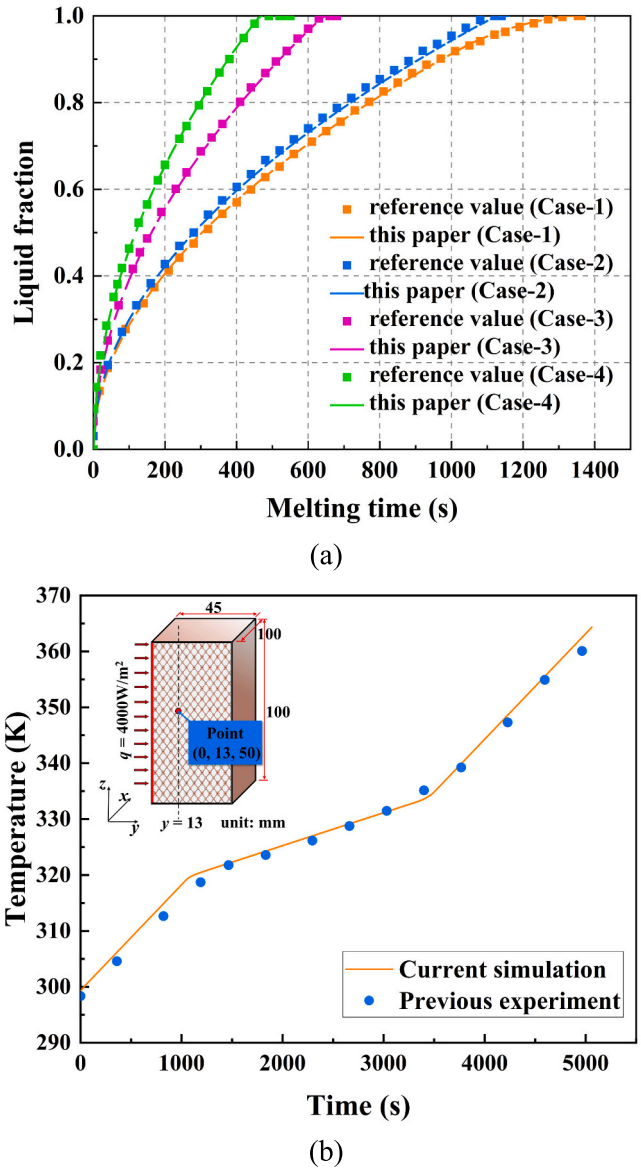

Fig. 6. Model validation results under the configuration of fully metal foam filled [45] (a) and comparison with experimental data of Li et al. [46] (b).

transfer proceeds by natural convection and buoyancy. With further melting, the liquid reaches the right wall, and the liquid-solid interface moves downward. Complete melting occurs in 3180 s.

For fully filled metal foam in paraffin, the liquid-solid interface is initially vertical, developing close to the left heating surface. This is explained by heat transfer through conduction and by the fact that natural convection is highly weakened by the porous structure of the metal foam. Remarkably, the thermal conductivity of the composite increases to 14.2 W/(m K) according to the Bhattacharya model (Eq. (2)) after the addition of the metal foam. In addition, complete melting time occurs in 93 s, which is 97 % lower than for the pure paraffin, confirming the improvement of the system thermal conductivity by adding metal foam.

For these two cases, the temperature distribution of the melting process is shown in Fig. 9. For the pure paraffin, the monitoring points O_1, O_2, O_3 and O_4 reached the phase-transition temperature of 318.15 K in 443 s, 1179 s, 1880 s and 2674 s, respectively. O_1 reached first 318.15 K because, in the initial stage of melting, the liquid paraffin moved upward under the buoyancy, resulting liquefaction of the paraffin at the top. The temperature response time of paraffin increased with the deepening of the location of the monitoring points, showing a "ladder" distribution. The reason is that the high-temperature liquid paraffin was floating at the top, while the solid paraffin at the bottom was slow in phase transition due to low thermal conductivity. Compared with O_1, the time for O_4 to reach 318.15 K increased by 5 times, and the temperature distribution inside the pure paraffin was highly heterogeneous.

For the metal foam fully filling the system, the time for O_1, O_2, O_3 and O_4 to reach 318.15 K is 17 s, 24.1 s, 29.5 s, 37.4 s, respectively. The time of O_1 reaching phase transition temperature is 96.2 % less than that of the pure paraffin system. This is explained by the high thermal conductivity of the metal foam. According to the hysteresis of response time, the natural convection effect of liquid paraffin is weakened but does not disappear completely in the foam metal. Moreover, the "ladder" distribution observed for the pure paraffin disappears and the temperature distribution almost becomes linear, which indicates that the addition of metal foam improves the uniformity of temperatures, and changes the main mode of heat transfer from natural convection to heat conduction.

4.2. *Partially-filled systems*

4.2.1. *Liquid-solid interface development*

Fig. 10 shows the evolution of the liquid-solid interface of the bottom-filled and top-filled configurations. For the bottom-filled configuration, at the top of the pure paraffin region, the flow is consistent with that of the unfilled configuration (Fig. 7). However, in the metal foam-paraffin region, the heat conduction is enhanced by the metal foam. Indeed, the high thermal metal conductivity reduces the thermal resistance and accelerates paraffin melting. As a consequence, the liquid-solid interface moves much faster to the right. Then, accumulation of heat on the right of the metal foam region induces an upward climb of heat toward and in the pure paraffin region by natural convection, as shown by the peak-shaped curves on the right. This consistent with the phenomenon observed by Wang et al. [37] Interestingly, as ξ increases from 0.25 to 0.75, the curvature of the liquid-solid interface increases and the natural convection appears to become more intense in the pure paraffin region. This is probably caused by the

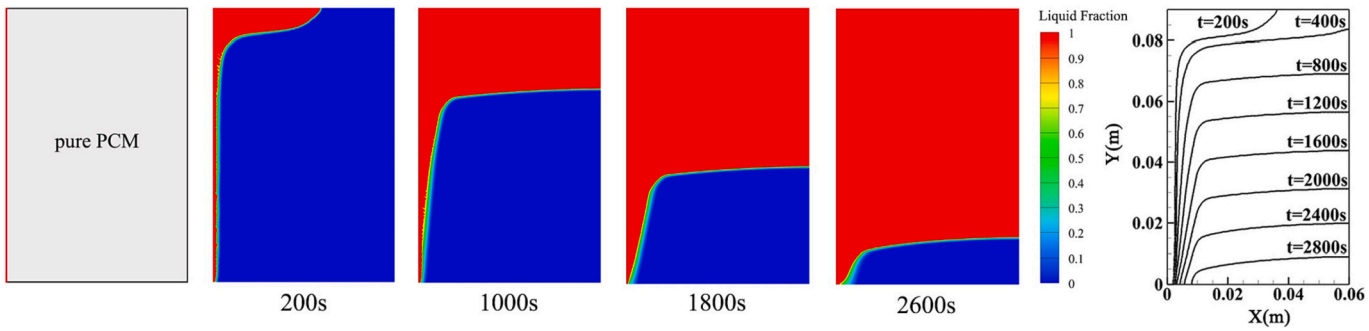

Fig. 7. Evolution of the liquid-solid interface in a system containing a pure PCM (paraffin), with height ratio ξ of 0.

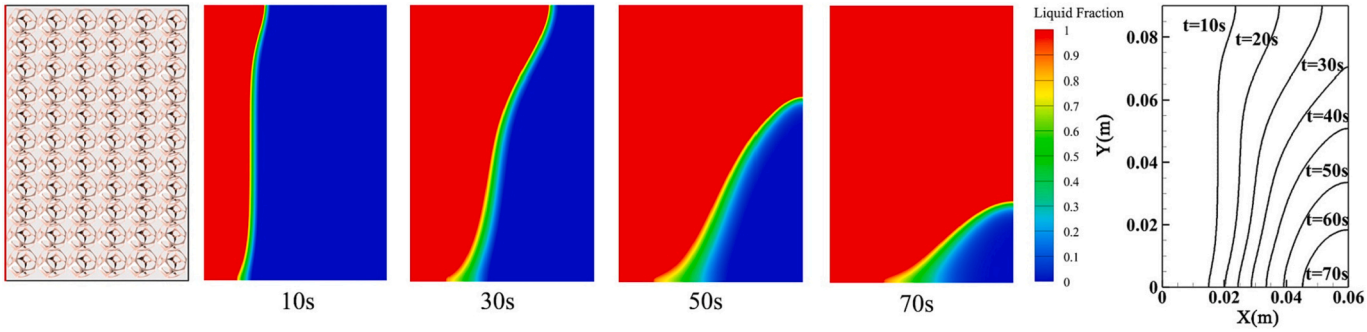

Fig. 8. Evolution of the liquid-solid interface in a system containing a PCM (paraffin) fully filled with metal foam, with height ratio ξ of 1.

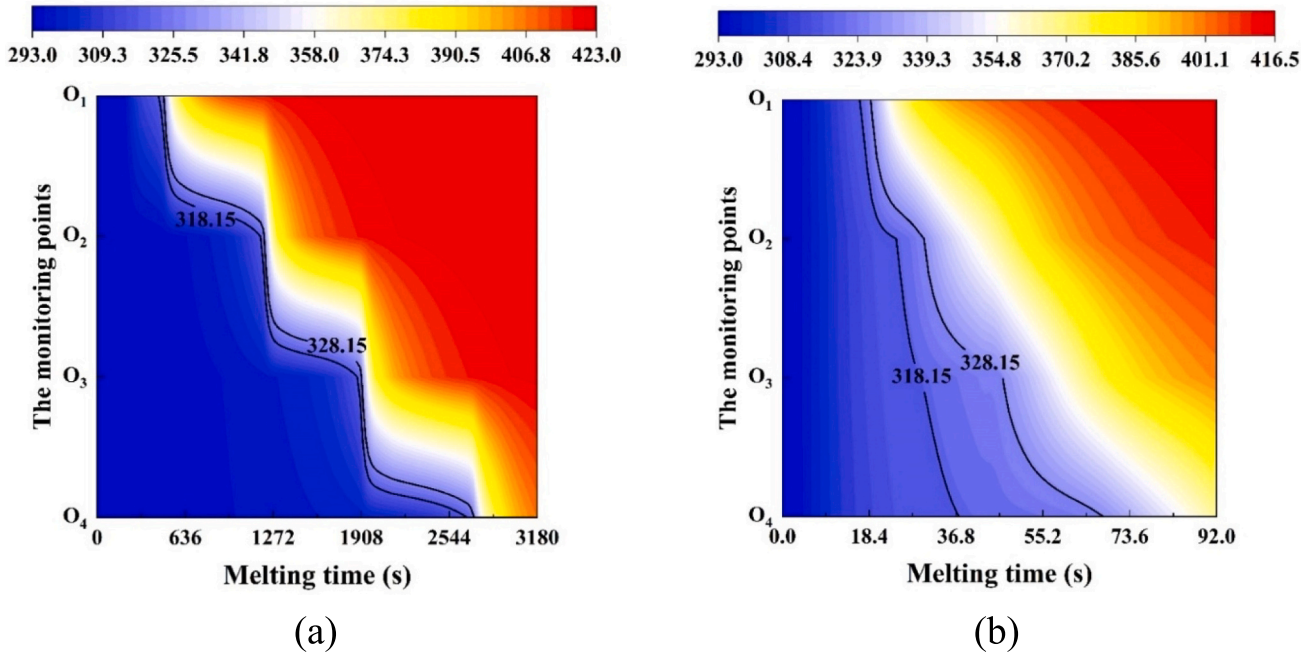

Fig. 9. The distribution of temperature during the melting period: (a) ξ = 0; (b) ξ = 1.

lower amount of paraffin, accelerating the combination of convection surfaces. This is demonstrated in Fig. 11, where the flow velocity in the pure paraffin region of the bottom-filled configuration has an order of magnitude higher velocity.

Contrastingly, for the top-filled configuration, the liquid-solid interface development in the pure paraffin and in the composite regions is similar to the unfilled and fully-filled configurations, respectively (Figs. 7 and 8). The liquid-solid interface moves right and very rapidly in the metal foam region, but moves upward and much more slowly in the pure paraffin region. Compared to the bottom-filled configuration, there is less heat transfer between the two regions, as can be confirmed in Table 5. Table 5 presents the average heat flux (q) at the interface between pure paraffin and composite region, where t* = 0.5 (t* = t/tm), calculated by Eqs. (10)–(12). Where W is the width of LHTES, λ_{co} represents the comprehensive thermal conductivity of the local filling material, and $gradT_i$ is the temperature gradient at the interface.

$$q = \frac{1}{W}\sum_{i=1}^{n} q_i W_i \tag{10}$$

$$q_i = -\lambda_{co} gradT_i \tag{11}$$

$$\lambda_{co} = \xi H\lambda_{eff} + (1-\xi)H\lambda_{pcm} \tag{12}$$

In addition, cusps and discontinuous occur at the phase transformation boundary of the regional interface, because due to the addition of metal foam, the composite region melts more rapidly, which makes the melting rate of the two regions unbalanced, and leads to significant changes in the interface shape of liquid-solid PCM at the junction of the pure paraffin and the metal foam-paraffin composite region. Poulikakos et al. [47] observed similar phenomenon in their study.

4.2.2. *Temperature analysis*

Fig. 12 displays the influence of different filling configurations on the internal temperature distribution. Taking the configuration with height ratio ξ of 0.5 as an example. For the top-filled configuration, the monitoring points reach 318.15 K in the order of O_1, O_2, O_3 and O_4, in 17 s, 29 s, 381 s and 1193 s, respectively. By contrast, for the BFC, the order is O_3, O_4, O_1 and O_2, in 18 s, 30 s, 424 s and 925 s, respectively. The complete melting time of PCM in the bottom-filled configuration is 36.39 % shorter than that in the top-filled configuration.

In the metal foam-paraffin region, the temperature responses of O_1 and O_2 in Fig. 12b and O_3 and O_4 in Fig. 12e are rapid, indicating that the metal foam improves the thermal conductivity in the composite region. However, the response time of O_4 in the bottom-filled configuration is 67 % higher than that of O_3, and that of O_2 in the top-filled

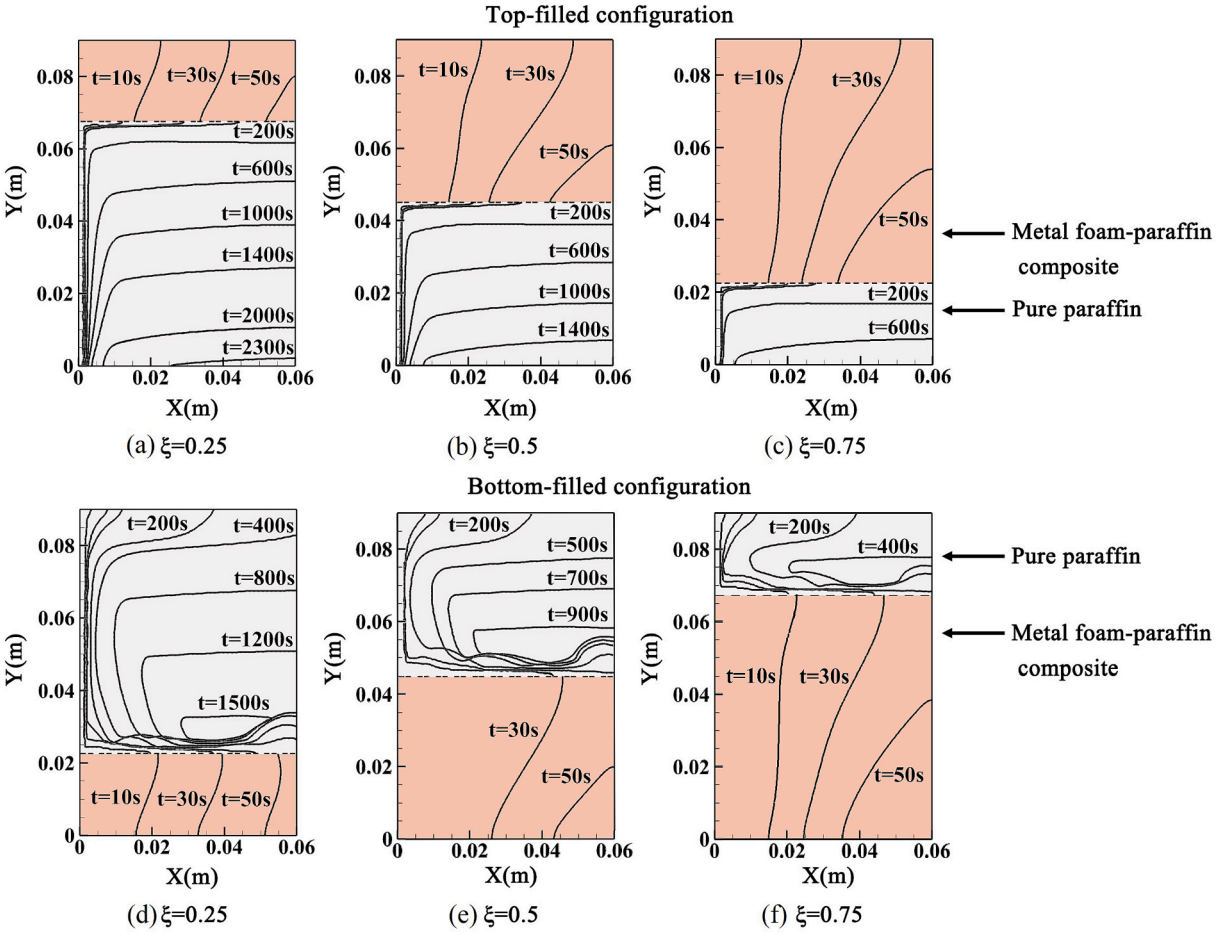

Fig. 10. Liquid-solid interface development with top filling (a)–(c) and bottom filling (d)–(f) configurations. Pure paraffin in grey, metal foam-paraffin composite in pink. (For interpretation of the references to colour in this figure legend, the reader is referred to the web version of this article.)

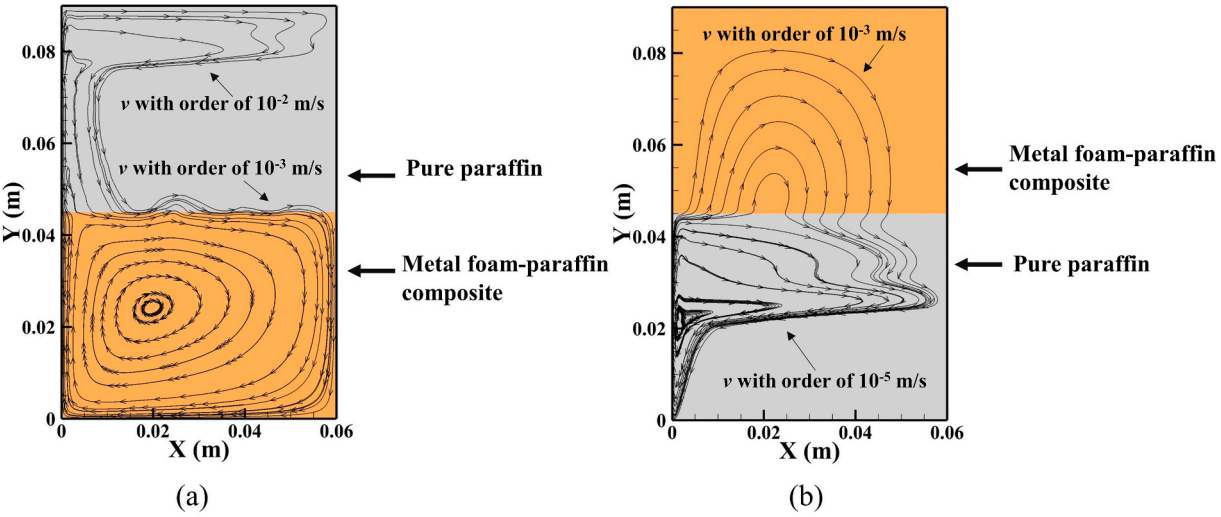

Fig. 11. Flow characteristics of bottom filling (a) and top filling (b) configurations for ξ = 0.5 (t* = 0.5).

configuration is 47 % higher than that of O_1. The time difference of temperature rise between these two points indicates that the natural convection of liquid PCM is not completely inhibited in the metal foam. In addition, when the bottom is filled with metal foam, the high-temperature liquid PCM is driven by buoyancy, which leads to more heat energy transfer to the upper portion, thus hindering the melting of the composite region. This is explaining why the difference in temperature response time between the two points is larger.

In the pure paraffin region, the monitoring point was always slower to reach 318.15 K than in the composite region. This implies that natural convection is the main heat transfer mechanism in the melting process of pure PCM. The response time difference of O_3 and O_4 was 812 s in

Table 5
Average heat flux at the interface between pure paraffin and composite region (t* = 0.5).

	ξ = 0.25, q (W m^{-2})	ξ = 0.5, q (W m^{-2})	ξ = 0.75, q (W m^{-2})
Top-filled configuration	470.3	3036.4	5570.1
Bottom-filled configuration	3026.5	7779.5	13,178.6

Fig. 12b, while the response time difference of O_1 and O_2 was 501 s in Fig. 12e. From the large time difference, it can be concluded that the natural convection in the pure paraffin region is more intense under the bottom-filled configuration. Natural convection occurs both at the top of the pure paraffin region and at the region interface, and the PCM is aided by two forces that accelerate the melting process.

For the top-filled configuration, when ξ increases from 0.25 to 0.75, O_4 is the last point reaching 318.15 K, in 1931 s, 1193 s, and 406 s, respectively. With the increase of the amount of metal foam, the melting time is further reduced by the strengthening of heat conduction. Concurrently, this will further inhibit the natural convection of liquid PCM, which can be explained by Fig. 12a–c: the number of steps decreases with increasing ξ. For the bottom-filled configuration, when ξ increases from 0.25 to 0.75, the last point reaching 318.15 K is O_3, O_2, O_1, in 925 s, 424 s, 372 s. Compared with the top-filled configuration, this time was shortened by 52.1 %, 64.5 % and 8.3 %, respectively. Therefore, when the same amount of metal foam is added, the bottom-filled configuration favors natural convection and therefore melts faster. Last, the uniformity of the temperature distribution increases with increasing ξ, regardless of the filling configuration.

4.2.3. *Liquid fraction and prediction formulas*

Fig. 13 displays the influence of different regions in bottom filling and top filling configurations on liquid fraction. For the pure paraffin region, the liquid fraction of the bottom filling configuration is higher and develops more rapidly compared to the top filling configuration. As the filling height ratio ξ increased from 0.25 to 0.75, the melting time of the bottom-filled configuration was shortened by 36.4 %, 41.4 % and 48.8 % compared with that of the top-filled configuration, respectively. In addition, the liquid fraction of bottom-filled configuration increases steadily at the beginning of the melting process. However, with time, the slopes increase significantly, which means that the natural convection in the pure paraffin rises gradually. For the top-filled configuration, the slope of the liquid fraction is almost constant, indicating that the natural convection of the liquid PCM is maintained at a low level, which can also be verified by the velocity field analysis described earlier.

For the metal foam-paraffin region, the opposite phenomenon can be seen, where the liquid fraction of the top-filled configuration is higher than that of the bottom-filled configuration at any time. Combined with the velocity field analysis, it can be seen that in this region, the melting rate is higher in the whole melting period when the top is filled with metal foam. Compared with the bottom-filled configuration, the melting time is reduced by 27.4 %, 12.3 % and 6.9 %, respectively. In addition, it is found that when the filling height ratio ξ is equal, the shortening rate of melting time in the composite region decreases greatly, because the heat transfer mechanism in the composite region is mainly heat conduction. Since the heat loss caused by natural convection is not dominant, the melting time difference between the two configurations in this region is not large. However, in the pure paraffin region, natural convection becomes the main heat transfer mechanism, so natural convection is particularly important, and its contribution to shortening the melting time is greater. In general, when the metal foam is at the bottom, its melting time is less than that of the top filling.

In order to better manage the LHTES system in practical application, it is necessary to obtain the melting degree of PCM quickly. Based on literature review [48,49], the liquid fraction of metal foam-paraffin

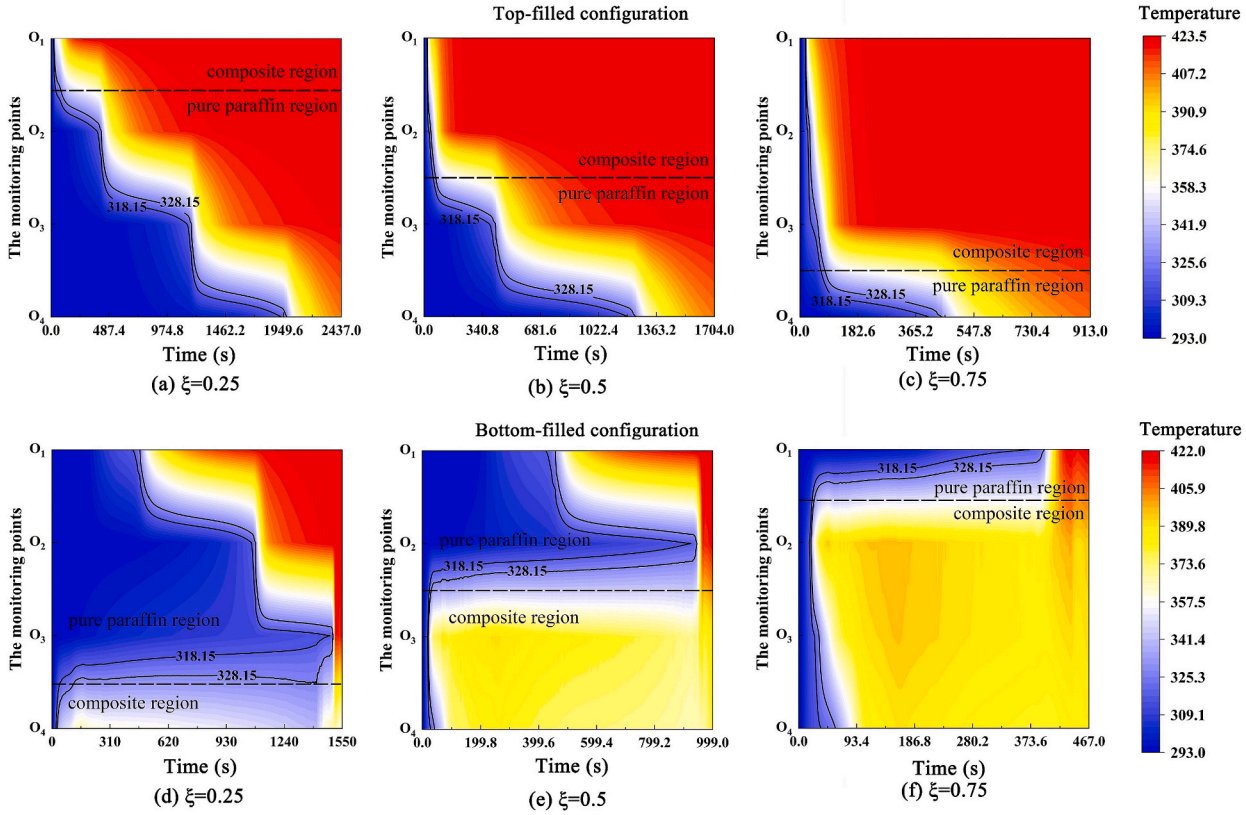

Fig. 12. The distribution of temperature field during the melting period: (a)–(c) top-filled configuration; (d)–(f) bottom-filled configuration.

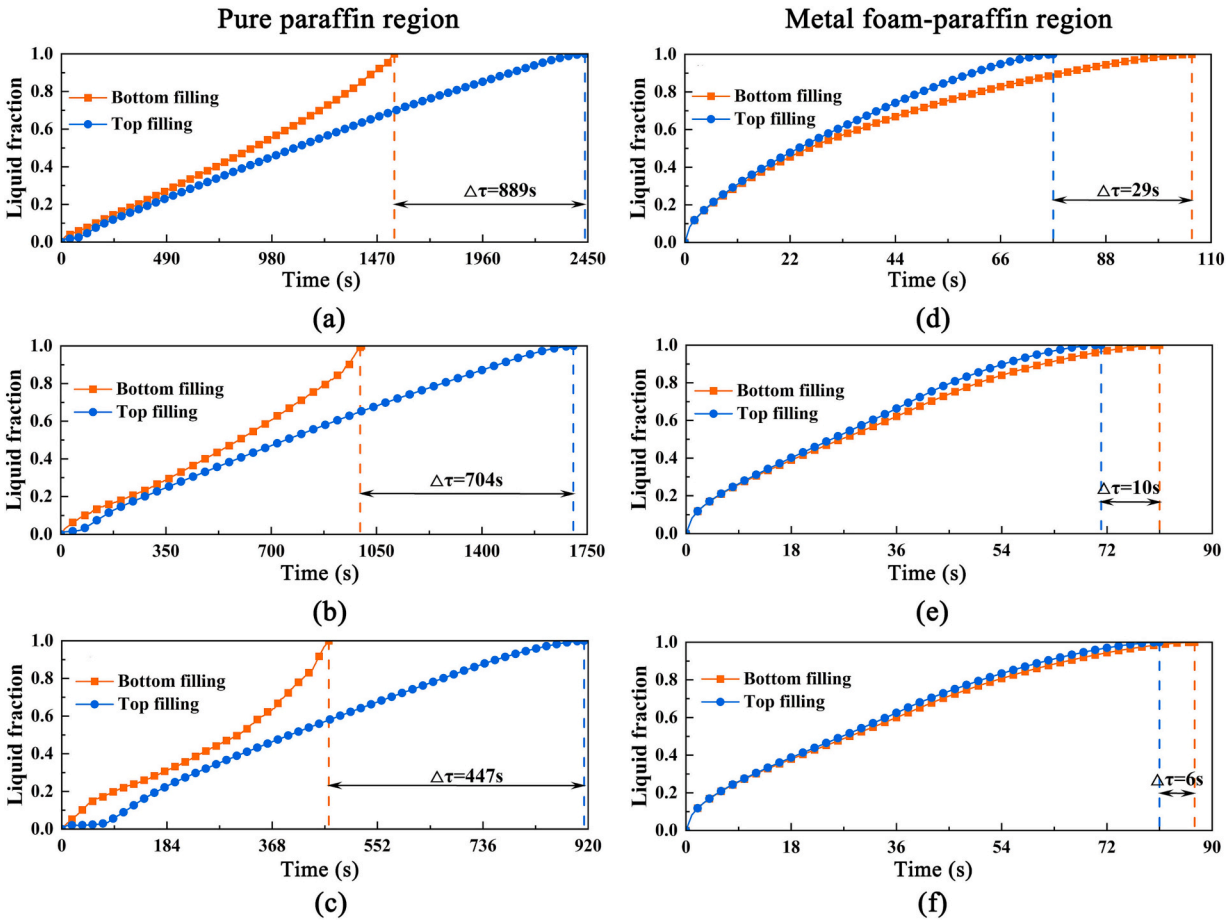

Fig. 13. Influence of the different filling configurations on the liquid fraction with pure paraffin regions: (a) ξ = 0.25; (b) ξ = 0.5; (c) ξ = 0.75 and metal foam-paraffin regions: (d) ξ = 0.25; (e) ξ = 0.5; (f) ξ = 0.75.

composite materials can generally be written as the following formula in a dimensionless form:

$$\beta = \sum a_i (SteFoRa^n)^{m_i} \tag{13}$$

$$Fo = \frac{\alpha t}{H^2}, Ste = \frac{C_p(T_w - T_m)}{L_a}, Ra = \frac{g\gamma L^3(T_w - T_m)}{\nu\alpha} \tag{14}$$

where *Fo* is Fourier number and represents the dimensionless time of the unsteady heat transfer process. *Ste* is Stefan number, defined as the ratio of sensible heat to latent heat. *Ra* is Rayleigh number, which is used to measure the strength of natural convection. a_i, n and m_i are determined according to different LHTES units. *H* is the height of the LHTES unit. *L* is the characteristic length, and the height of the pure paraffin region is taken in this study.

Since the partially filled configuration results in the melting imbalance between the pure paraffin region and the composite region, the liquid fraction of the two regions was analyzed separately by dimensionless analysis. This allows a more accurate description of the melting degree of the LHTES system. The dimensionless analysis was carried out under different filling configurations, and the variable was the filling height ratio ξ. In this study, the *Ste* was a constant and was ignored. Figs. 14 and 15 show the dimensionless analysis of the liquid fraction under the bottom-filled and the top-filled configurations. Taking the bottom-filled configuration (Fig. 14) as an example, the relationship between the liquid fraction and the *Fo* is firstly analyzed. As can be seen from Fig. 14(a)–(b), for the pure paraffin region, when ξ increases from 0.25 to 0.75, the final value of *Fo* decreased sharply from 0.032 to 0.010. In contrast, in the composite region, it can be observed that the difference between *Fo* of different ξ is significantly shortened. This is mainly because the natural convection in the pure paraffin region is more intense, so it is necessary to take the *Ra* into account and modify the filling height ratio term for different filling configurations. According to the fitting results of Fig. 14(c)–(d), the liquid fraction can be well expressed by $FoRaf(\xi)$. After fitting, the liquid fraction prediction formula of the two filling configurations is shown as follows:

BFC-pure paraffin region:

$$\beta_1 = 1.37X - 1.78X^2 + 2.86X^3 - 1.09X^4$$

$$X = FoRa^{0.25} f_1(\xi), f_1(\xi) = 1.26 - 5.08\xi + 9.12\xi^2$$

BFC-composite region:

$$\beta_2 = 57.20X - 2.29 \times 10^3 X^2 + 5.77 \times 10^4 X^3 - 5.3 \times 10^5 X^4$$

$$X = FoRa^{0.25} f_2(\xi), f_2(\xi) = 0.08 + 2.09\xi - 1.39\xi^2$$

TFC-pure paraffin region:

$$\beta_3 = 0.83X + 1.55X^2 - 2.36X^3 + 1.00X^4$$

$$X = FoRa^{0.25} f_3(\xi), f_3(\xi) = 2.34 - 11.1\xi + 18.39\xi^2$$

TFC-composite region:

$$\beta_4 = 1.36 \times 10^2 X - 1.36 \times 10^4 X^2 + 8.94 \times 10^5 X^3 - 2.14 \times 10^7 X^4$$

$$X = FoRa^{0.25} f_4(\xi), f_4(\xi) = 0.34 + 0.23\xi + 0.82\xi^2$$

The above normalization formulas are reasonable under the

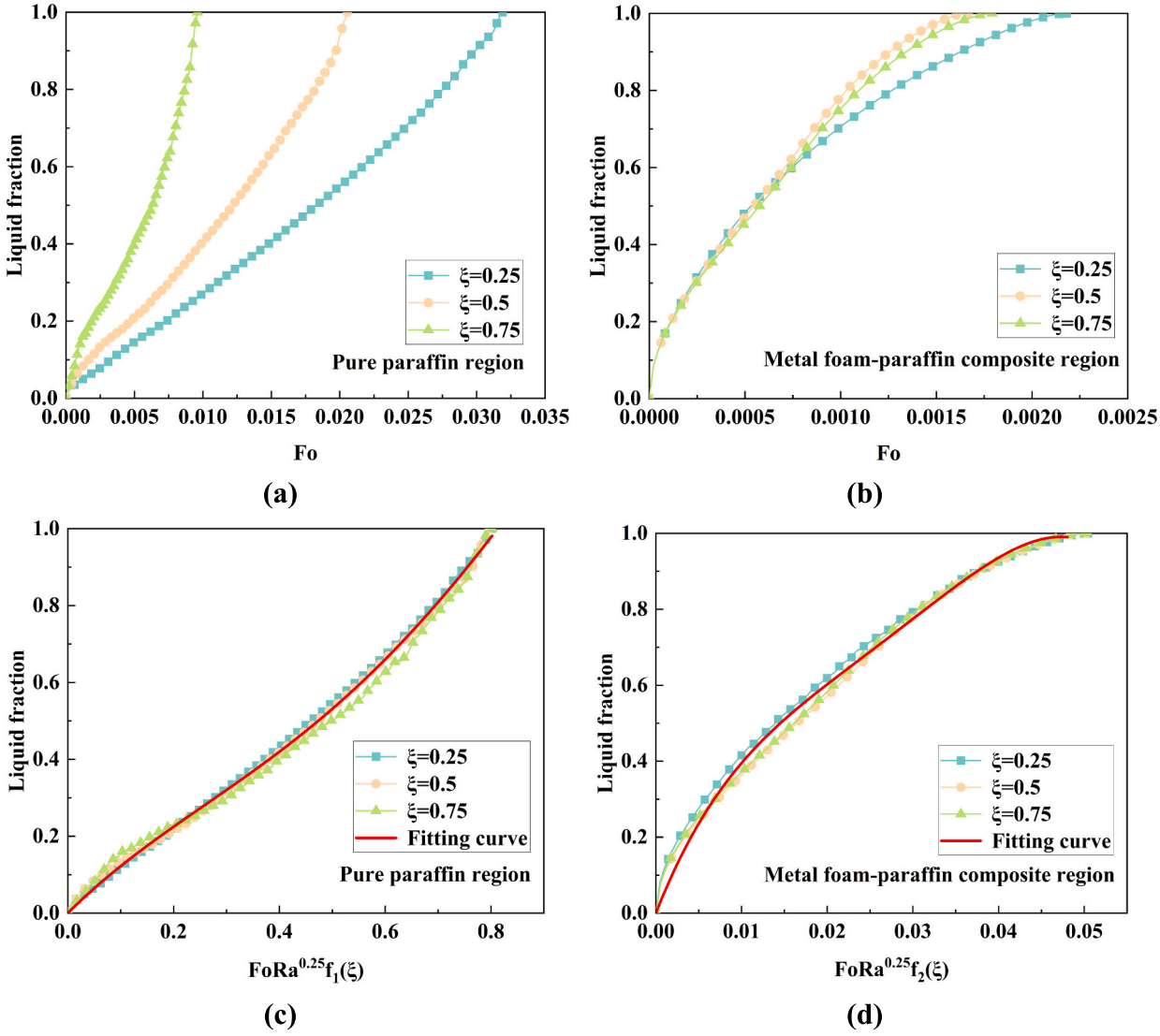

Fig. 14. Dimensionless analysis of liquid fraction in bottom filled configuration (BFC). Variation of liquid fraction with *Fo* in pure paraffin (a) and composite (b) regions. Variation of liquid fraction with *FoRaf*(ξ) in pure paraffin (c) and composite (d) regions.

geometric model studied in this paper within the parameter range: $0.25 \leq \xi \leq 0.75$, $2.22 \times 10^4 < Ra < 4.04 \times 10^6$, $0 < X < 0.035$, $0 < \beta < 1$. Compared with the numerical results, the maximum errors of β_1, β_2, β_3 and β_4 are 5.67 %, 23.00 %, 7.34 % and 6.58 %, respectively.

5. Conclusion

In the current study, for the heat storage unit of LHTES system, two types of filling modes, top filling configuration and bottom filling configuration, are designed. Meanwhile, the different filling height ratio (ξ) of the metal foam is considered. The melting characteristics of different LHTES units were analyzed. Conclusions can be summarized as follows:

(1) By comparing unfilled and fully filled cases, it is found that the addition of metal foam can significantly enhance the heat conduction of paraffin wax, increase the melting rate of paraffin wax, and improve the uniformity of temperature distribution of composite materials. But it also inhibits the natural convection of liquid paraffin.

(2) In the pure paraffin region, the natural convection of liquid paraffin in the bottom-filled configuration is more intense than that in the top-filled configuration, so that the solid paraffin in the bottom-filled configuration can reach the phase transition temperature faster and melt. The reverse is true in the composite region, where the melting rate of the bottom-filled configuration is slower due to heat escape.

(3) At the junction of pure paraffin region and composite region, cusp and discontinues occurred on the liquid-solid interface. It is mainly because the high thermal conductivity of the metal foam makes the melting rate of the composite region rise sharply, which causes the melting imbalance between the two regions.

(4) Through the dimensionless analysis of the melting period of the metal foam-paraffin composite system, it is shown that the liquid fraction is an essential parameter related to *Fo*, *Ra* and ξ under the condition studied in this paper. The liquid fraction prediction formula fitted in this paper can help to quickly obtain the melting degree of LHTES units in engineering applications.

CRediT authorship contribution statement

Wang Hui: Writing - Original Draft, Conceptualization, Project administration. **Ying Qifan**: Conceptualization, Methodology, Software, Data, Visualization. **Eric Lichtfouse**: Writing - Review & Editing. **Hu**

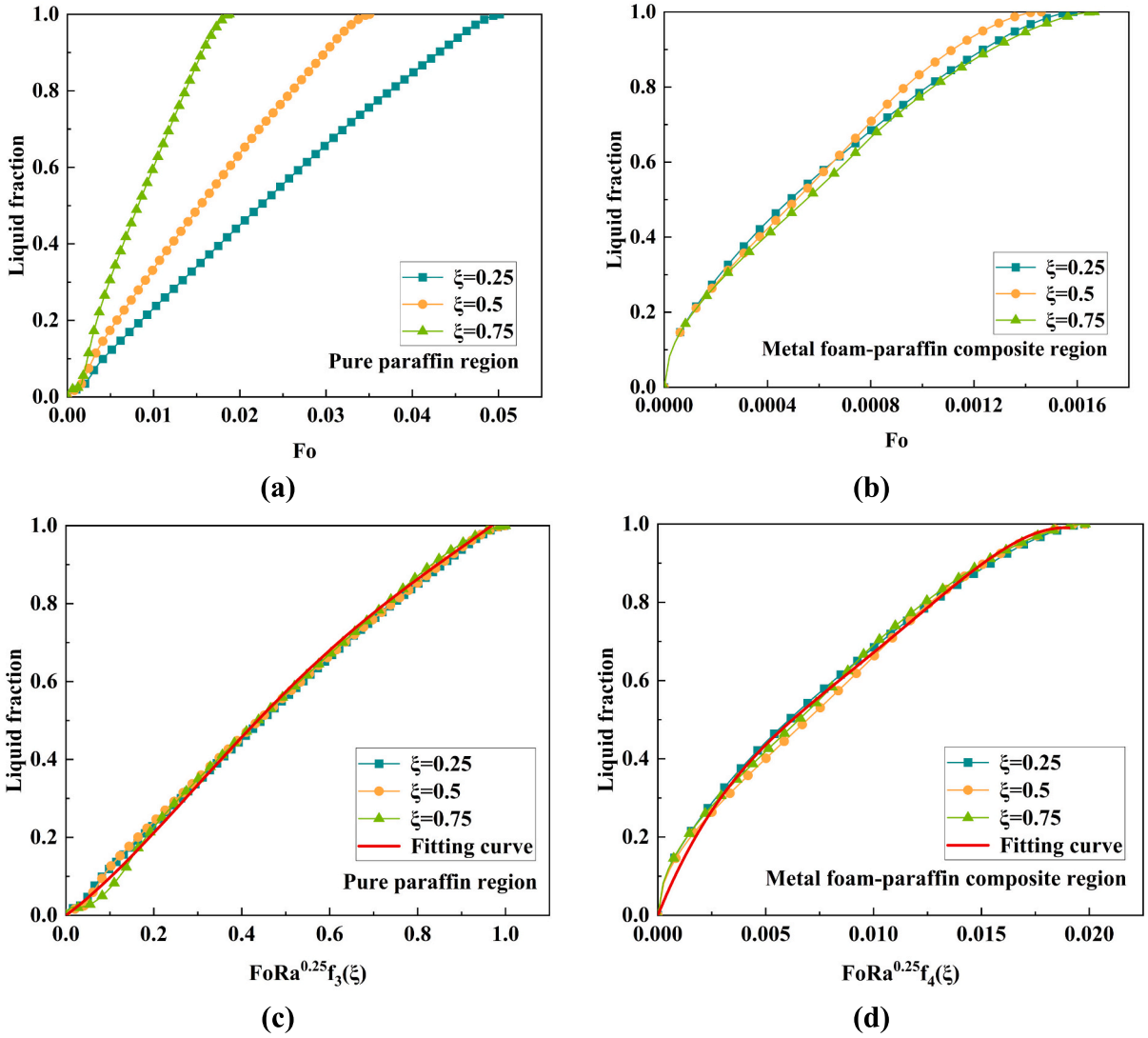

Fig. 15. Dimensionless analysis of liquid fraction in top filled configuration (TFC). Variation of liquid fraction with *Fo* in pure paraffin (a) and composite (b) regions. Variation of liquid fraction with $FoRaf(\xi)$ in pure paraffin (c) and composite (d) regions.

Zexu: Resources, Supervision. **Diao Yongfa**: Resources, Supervision.

Declaration of competing interest

The authors declare that they have no known competing financial interests or personal relationships that could have appeared to influence the work reported in this paper.

Data availability

The data that has been used is confidential.

Acknowledgments

The study was funded by State Key Laboratory for Modification of Chemical Fibers and Polymer Materials, Donghua University (KF2123), Shanghai Sailing Program (19YF14011700).

References

[1] S.K. Shukla, P. Rathore, Potential of microencapsulated pcm for energy savings in buildings: a critical review, Sustain. Cities Soc. 53 (2019), 101884.
[2] B. Ahmad, M. Irfan, S. Salem, et al., Energy efficiency in the post-covid-19 era: exploring the determinants of energy-saving intentions and behaviors, Front. Energy Res. 9 (2022), 824318.
[3] Y. Gao, X. Zhang, X. Xu, et al., Application and research progress of phase change energy storage in new energy utilization, J. Mol. Liq. 343 (2021), 117554.
[4] X.Y. Tang, P.Y. Dou, Z.Q. Dai, et al., Structural design and analysis of a solar thermochemical reactor partially filled with phase change material based on shape optimization, Sol. Energy 236 (2022) 613–625.
[5] S.H. Tan, X.L. Zhang, Progress of research on phase change energy storage materials in their thermal conductivity, J. Energy Storage 61 (2023), 106772.
[6] X. Lin, X. Zhang, Research progress of phase change storage material on power battery thermal management, Energy Technol. 9 (4) (2021) 2000940.
[7] J. Luo, D. Zou, Y. Wang, et al., Battery thermal management systems (btms) based on phase change material (pcm): a comprehensive review, Chem. Eng. J. 430 (2022), 132741.
[8] E. Elnajjar, Using pcm embedded in building material for thermal management: performance assessment study, Energy Build. 151 (2017) 28–34.
[9] Y. Wang, X. Zhang, J. Ji, et al., Thermal conductivity modification of n-octanoic acid-myristic acid composite phase change material, J. Mol. Liq. 288 (2019), 111092.
[10] B.E. Jebasingh, A.V. Arasu, A comprehensive review on latent heat and thermal conductivity of nanoparticle dispersed phase change material for low-temperature applications, Energy Storage Mater. 24 (2020) 52–74.
[11] B. Lu, Y. Zhang, D. Sun, et al., Experimental investigation on thermal behavior of paraffin in a vertical shell and spiral fin tube latent heat thermal energy storage unit, Appl. Therm. Eng. 187 (2021), 116575.
[12] Z.J. Zheng, Y. Sun, Y. Chen, et al., Study of the melting performance of shell-and-tube latent heat thermal energy storage unit under the action of rotating finned tube, J. Energy Storage 62 (2023), 106801.

[13] M.K. Pasupathi, K. Alagar, M. Mm, et al., Characterization of hybrid-nano/paraffin organic phase change material for thermal energy storage applications in solar thermal systems, Energies 13 (19) (2020) 5079.
[14] Y. Han, Y. Yang, T. Mallick, et al., Nanoparticles to enhance melting performance of phase change materials for thermal energy storage, Nanomaterials 12 (11) (2022) 1864.
[15] G. Chen, Y. Su, D. Jiang, et al., An experimental and numerical investigation on a paraffin wax/graphene oxide/carbon nanotubes composite material for solar thermal storage applications, Appl. Energy 264 (2020), 114786.
[16] Y. Lin, Q. Kang, H. Wei, et al., Spider web-inspired graphene skeleton-based high thermal conductivity phase change nanocomposites for battery thermal management, Nano-Micro Lett. 13 (1) (2021) 1–14.
[17] H. Wang, L.J. Guo, K. Chen, Theoretical and experimental advances on heat transfer and flow characteristics of metal foams, SCIENCE CHINA Technol. Sci. 63 (5) (2020) 705–718.
[18] A. Mirshekar, M.R. Goodarzi, D. Mohebbi-Kalhori, et al., Experimental study of heat transfer enhancement using metal foam partially filled with phase change material in a heat sink, J. Energy Storage 60 (2023), 106496.
[19] D. Zou, X. Ma, X. Liu, et al., Thermal performance enhancement of composite phase change materials (pcm) using graphene and carbon nanotubes as additives for the potential application in lithium-ion power battery, Int. J. Heat Mass Transf. 120 (2018) 33–41.
[20] A. Farzanehnia, M. Khatibi, M. Sardarabadi, et al., Experimental investigation of multiwall carbon nanotube/paraffin based heat sink for electronic device thermal management, Energy Convers. Manag. 179 (2019) 314–325.
[21] Y. Tian, C.Y. Zhao, A numerical investigation of heat transfer in phase change materials (pcms) embedded in porous metals, Energy 36 (9) (2011) 5539–5546.
[22] Z. Liu, Y. Yao, H. Wu, Numerical modeling for solid–liquid phase change phenomena in porous media: Shell-and-tube type latent heat thermal energy storage, Appl. Energy 112 (dec.) (2013) 1222–1232.
[23] W.Q. Li, Z.G. Qu, Y.L. He, et al., Experimental study of a passive thermal management system for high-powered lithium ion batteries using porous metal foam saturated with phase change materials, J. Power Sources 255 (Jun.1) (2014) 9–15.
[24] M. Alipanah, X. Li, Numerical studies of lithium-ion battery thermal management systems using phase change materials and metal foams, Int. J. Heat Mass Transf. 102 (2016) 1159–1168.
[25] M. Martinelli, F. Bentivoglio, A. Caron-Soupart, et al., Experimental study of a phase change thermal energy storage with copper foam, Appl. Therm. Eng. 101 (2016) 247–261.
[26] P. Zhang, Z.N. Meng, H. Zhu, et al., Melting heat transfer characteristics of a composite phase change material fabricated by paraffin and metal foam, Appl. Energy 185 (pt.2) (2015) 1971–1983.
[27] W. Li, R. Hou, H. Wan, et al., A new strategy for enhanced latent heat energy storage with microencapsulated phase change material saturated in metal foam, Sol. Energy Mater. Sol. Cells 171 (2017) 197–204.
[28] Y. Yao, H. Wu, Thermal transport process of metal foam/paraffin composite (mfpc) with solid-liquid phase change: an experimental study, Appl. Therm. Eng. 179 (2020), 115668.
[29] Y. Tao, Y. You, Y. He, Lattice boltzmann simulation on phase change heat transfer in metal foams/paraffin composite phase change material, Appl. Therm. Eng. 93 (2016) 476–485.
[30] X. Meng, L. Yan, J. Xu, et al., Effect of porosity and pore density of copper foam on thermal performance of the paraffin-copper foam composite phase-change material, Case Stud. Therm. Eng. 22 (2020), 100742.
[31] S.Q. Zhang, L. Pu, S. Mancin, et al., Role of partial and gradient filling strategies of copper foam on latent thermal energy storage: an experimental study, Energy 255 (2022), 124517.
[32] A.H. Liu, J.J. Lin, Y.J. Zhuang, Piv experimental study on the phase change behavior of phase change material with partial filling of metal foam inside a cavity during melting, Int. J. Heat Mass Transf. 187 (2022), 122567.
[33] Z.Q. Zhu, Y.K. Huang, N. Hu, et al., Transient performance of a pcm-based heat sink with a partially filled metal foam: effects of the filling height ratio, Appl. Therm. Eng. 128 (2017) 966–972.
[34] Y.J. Hou, H. Chen, X.X. Liu, Experimental study on the effect of partial filling of copper foam on heat storage of paraffin-based pcm, Renew. Energy 192 (2022) 561–571.
[35] H. Zuo, M. Wu, K. Zeng, et al., Numerical investigation and optimal design of partially filled sectorial metal foam configuration in horizontal latent heat storage unit, Energy 237 (2021), 121640.
[36] X. Yang, Z. Niu, J. Guo, et al., Melting evaluation of a thermal energy storage unit with partially filled metal foam, Int. J. Energy Res. 46 (1) (2022) 195–211.
[37] Z. Wang, H. Zhang, B. Dou, et al., Effect of copper metal foam proportion on heat transfer enhancement in the melting process of phase change materials, Appl. Therm. Eng. 201 (2022), 117778.
[38] V. Joshi, M.K. Rathod, Thermal performance augmentation of metal foam infused phase change material using a partial filling strategy: an evaluation for fill height ratio and porosity, Appl. Energy 253 (2019), 113621.
[39] H. Zheng, C. Wang, Q. Liu, et al., Thermal performance of copper foam/paraffin composite phase change material, Energy Convers. Manag. 157 (2018) 372–381.
[40] A. Chamkha, A. Veismoradi, M. Ghalambaz, et al., Phase change heat transfer in an l-shape heatsink occupied with paraffin-copper metal foam, Appl. Therm. Eng. 177 (2020), 115493.
[41] X. Xiao, P. Zhang, Numerical and experimental study of heat transfer characteristics of a shell-tube latent heat storage system: part i–charging process, Energy 79 (2015) 337–350.
[42] J.G. Fourie, J.P. Du Plessis, Pressure drop modelling in cellular metallic foams, Chem. Eng. Sci. 57 (14) (2002) 2781–2789.
[43] V.V. Calmidi, Transport Phenomena in High Porosity Fibrous Metal Foams, University of Colorado at Boulder, 1998.
[44] A. Bhattacharya, V.V. Calmidi, R.L. Mahajan, Thermophysical properties of high porosity metal foams, Int. J. Heat Mass Transf. 45 (2002) 1017–1031.
[45] Z.J. Zheng, C. Yang, Y. Xu, et al., Effect of metal foam with two-dimensional porosity gradient on melting behavior in a rectangular cavity, Renew. Energy 172 (2021) 802–815.
[46] W.Q. Li, Z.G. Qu, Y.L. He, et al., Experimental and numerical studies on melting phase change heat transfer in open-cell metallic foams filled with paraffin, Appl. Therm. Eng. 37 (2012) 1–9.
[47] D. Poulikakos, A. Bejan, Natural convection in vertically and horizontally layered porous media heated from the side, Int. J. Heat Mass Transf. 26 (12) (1983) 1805–1814.
[48] C.J. Ho, R. Viskanta, Heat transfer during melting from an isothermal vertical wall, J. Heat Transf. 106 (1) (1984) 12–19.
[49] V. Shatikian, G. Ziskind, R. Letan, Numerical investigation of a pcm-based heat sink with internal fins: constant heat flux, Int. J. Heat Mass Transf. 51 (5–6) (2008) 1488–1493.